LHCb's Sensitivity to New CP-Violating Phases in the Decay $\mathrm{B_s^0} \to \phi\phi$

Public Note

Issue: 1
Revision: 0

Reference: LHCb 2007-047
Created: May 2007
Last modified: May 29, 2007

Authors: Sandra Amato[a], Judith McCarron[b], Franz Muheim[b], Bruno Souza de Paula[a], Yuehong Xie[b]

[a] Federal University of Rio de Janeiro, UFRJ, Rio de Janeiro, Brasil
[b] University of Edinburgh, Edinburgh EH9 3JZ, United Kingdom

Abstract

This note describes the selection of the $\mathrm{B}_\mathrm{s}^0 \to \phi(\mathrm{K}^+\mathrm{K}^-)\phi(\mathrm{K}^+\mathrm{K}^-)$ decay channel in LHCb experiment using data produced in Monte Carlo simulation. We expect about 3.1 k signal events in $2\,\mathrm{fb}^{-1}$ of data with an upper limit on the background to signal ratio, $B/S < 0.8$ at 90% CL. We also present the sensitivity of this channel to new physics. There are two approaches to test the Standard Model (SM) using this channel: measure the CP asymmetries in a model-independent way and compare them with their SM predictions; or simply assume the SM is valid, measure the total weak phase based on the SM and compare the measurement with the SM prediction. We adopt the latter for this study. The total weak phase can be measured to a statistical precision of 0.11 in $2\,\mathrm{fb}^{-1}$ of data and 0.05 in $10\ \mathrm{fb}^{-1}$ of data. This channel therefore provides a good opportunity to search for physics beyond the SM with new CP-violating phases.

Contents

1 Introduction and Motivation

The decay $\mathrm{B_s^0} \to \phi\phi$ is governed by the $b \to s$ penguin diagrams shown in Fig. 1 for the Standard Model (SM). This makes it a very sensitive probe of CP-violating phases in new physics (NP) beyond the SM.

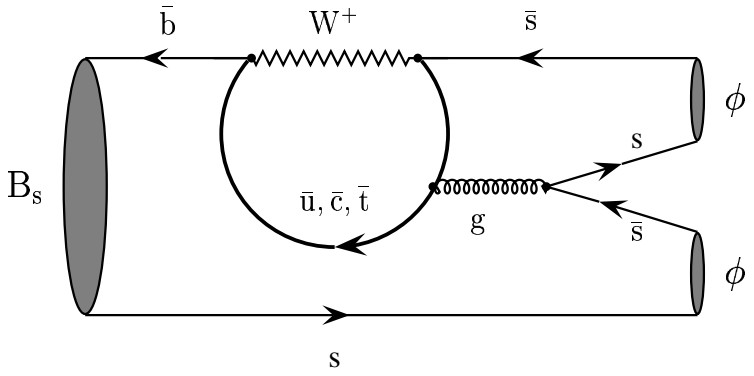

Figure 1 The lowest order SM diagrams contributing to the decay $\mathrm{B_s} \to \phi\phi$.

In $\mathrm{B_s^0}$ decays to an admixture of CP eigenstates, such as $\mathrm{B_s^0} \to \phi\phi$, CP violation can arise in the interference between mixing and decay. We first define our notation. The physical $\mathrm{B^0}$ mass eigenstates are:

$$|\mathrm{B_{H,L}}\rangle = \mathrm{p}|\mathrm{B^0}\rangle \mp \mathrm{q}|\overline{\mathrm{B}}^0\rangle \tag{1}$$

where the subscripts H and L stand for the "heavy" and the "light" $\mathrm{B^0}$ states which have masses $M_{H,L}$ and widths $\Gamma_{H,L}$. The interplay between mixing and decay is described by the following relation

$$\lambda_\mathrm{f} = \frac{\mathrm{q}}{\mathrm{p}}\frac{\bar{\mathrm{A}}_\mathrm{f}}{\mathrm{A}_\mathrm{f}} \tag{2}$$

where A_f and $\bar{A}_f$ are the decay amplitudes of a $\mathrm{B^0}$ or $\overline{\mathrm{B}}^0$ meson into a CP eigenstate f, respectively. CP violation in mixing or decay are expected to be negligible in this study, hence we only consider CP violation in the interference between mixing and decay. This is the case if

$$\left|\frac{\mathrm{q}}{\mathrm{p}}\right| = 1, \qquad \left|\frac{\bar{\mathrm{A}}_\mathrm{f}}{\mathrm{A}_\mathrm{f}}\right| = 1, \qquad \arg\lambda_\mathrm{f} \neq 0\ . \tag{3}$$

We define the phase Φ_M of $\mathrm{B^0}$ mixing as the argument of the off-diagonal element M_{12} of the mixing matrix

$$\mathrm{M_{12}} = |\mathrm{M_{12}}|\mathrm{e}^{\mathrm{i}\Phi_\mathrm{M}}\ . \tag{4}$$

The weak phase of the amplitude ratio $\frac{\bar{A}_f}{A_f}$ is called Φ_D. Note that Φ_M and Φ_D depend on phase conventions and cannot be measured separately. We find in the literature [1]

$$\lambda_\mathrm{f} = \pm\mathrm{e}^{-\mathrm{i}\Phi_\mathrm{M}}\frac{\bar{\mathrm{A}}_\mathrm{f}}{\mathrm{A}_\mathrm{f}} \tag{5}$$

where the $\pm$ sign is due to different phase conventions. However the phase of λ_f is an observable quantity as the convention dependent terms cancel when combining $\frac{q}{p}$ with the amplitude ratio. Hence the CP violating weak phases $\phi_\mathrm{s}(\mathrm{B_s^0} \to f) \equiv \Phi_\mathrm{M}(\mathrm{B_s^0}) - \Phi_\mathrm{D}(\mathrm{B_s^0} \to f)$ and

$\phi_{\rm d}({\rm B_d^0} \to f) \equiv \Phi_{\rm M}({\rm B_d^0}) - \Phi_{\rm D}({\rm B_d^0} \to f)$ are observables. For decays like ${\rm B_d^0} \to {\rm J/\psi K_S^0}$ and ${\rm B_s^0} \to {\rm J/\psi\phi}$ which are dominated by a tree level $b \to c\bar{c}s$ transition and which have a negligible weak phase $\Phi_{\rm D}$ in the decay amplitude ratio, we obtain

$$\begin{array}{ll} \phi_{\rm d}^{\rm SM}({\rm B_d^0} \to {\rm J/\psi K_S^0}) & = 2\beta \\ \phi_{\rm s}^{\rm SM}({\rm B_s^0} \to {\rm J/\psi\phi}) & = 2\ \arg(V_{ts}^* V_{tb}) = -2\chi = -2\eta\lambda^2 = -0.035 \end{array} \tag{6}$$

where η and λ are parameters in the Wolfenstein representation of the CKM matrix. Quantities with a "SM" superscript refer to their SM values.

In the SM, the CKM mechanism is the only source of flavour mixing and CP violation in the quark sector. Flavour Changing Neutral Currents (FCNC) are forbidden at tree level, and $b \to s$ quark transitions occur only via loop diagrams. The SM rates for FCNC decays of B mesons are very rare with typical branching ratios of $\mathcal{O}(10^{-6})$. These decays are sensitive to NP beyond the SM as new particles can enter the $b \to s$ penguin loop diagrams. NP could significantly alter the SM predictions for the $b \to s$ decay rate and CP violating asymmetries at experimentally observable levels. The time-dependent CP asymmetry in a hadronic $b \to s$ penguin decay can be compared with a decay based on a tree diagram which generally is insensitive to NP and which has the same weak phase. The B-factories measure the CP asymmetry $\sin 2\beta^{eff}$ in the decays ${\rm B_d^0} \to \phi{\rm K_S^0}$ and ${\rm B_d^0} \to \eta'{\rm K_S^0}$. A value of $\sin 2\beta^{eff}$ different from $\sin 2\beta$ measured in ${\rm B_d^0} \to {\rm J/\psi K_S^0}$ would signal physics beyond the SM. The current results indicate an intriguing deviation from the SM as all values are lower than expected. A naive average of several $b \to s$ penguin modes, which in principle should not be done because they may have different strong interaction corrections that generate different amount of CP asymmetries, indicates a 2.6σ discrepancy [2].

This method can also be applied to ${\rm B_s^0}$ mesons where one can measure the time dependent CP asymmetry in ${\rm B_s^0} \to {\rm J/\psi\phi}$ and ${\rm B_s^0} \to \phi\phi$. This will be exploited by LHCb.[1] New physics can enter into the ${\rm B_s^0}$–$\overline{\rm B}_{\rm s}^0$ mixing diagram and alter the mixing phase from its SM value by a NP phase $\Phi_{\rm M}^{NP}({\rm B_s^0})$. We use the following NP parameterisation in ${\rm B_s^0}$ mixing to define the NP mixing phase $\Phi_{\rm M}^{NP}$ and amplitude r_s

$$M_{12}^{\rm s\ NP} = M_{12}^{\rm s\ SM} r_{\rm s}^2 e^{i\Phi_{\rm M}^{\rm NP}} \ . \tag{7}$$

Thus the total weak phase measured in the time-dependent CP asymmetry of ${\rm B_s^0} \to {\rm J/\psi\phi}$ is

$$\phi_{\rm s}({\rm B_s^0} \to {\rm J/\psi\phi}) = \phi_{\rm s}^{\rm SM}({\rm B_s^0} \to {\rm J/\psi\phi}) + \Phi_{\rm M}^{\rm NP}({\rm B_s^0})\,. \tag{8}$$

Therefore the decay ${\rm B_s^0} \to {\rm J/\psi\phi}$ is very sensitive to new weak phases in ${\rm B_s^0}$ mixing.

In the hadronic penguin decay ${\rm B_s^0} \to \phi\phi$ there is a cancellation of the ${\rm B_s^0}$ mixing and decay phase in the SM [3]:

$$\begin{array}{ll} \phi_{\rm s}^{\rm SM}({\rm B_s^0} \to \phi\phi) & = -\arg\left(\eta_{\rm f}\lambda_{\rm f}\right) = -\arg\left(\eta_{\rm f}\frac{\rm q}{\rm p}\frac{\bar{\rm A}_{\rm f}}{\rm A_f}\right) = \Phi_{\rm M}^{\rm SM} - \Phi_{\rm D}^{\rm SM} \\ & \approx 2\ \arg(V_{\rm ts}^* V_{\rm tb}) - \arg(V_{\rm tb}V_{\rm ts}^*/V_{\rm tb}^* V_{\rm ts}) = -2\chi + 2\chi = 0\,. \end{array} \tag{9}$$

where $\eta_f = \pm 1$ are the CP eigenvalues which correspond to the CP-even and odd components of the decay. The contributions of the u and c quark in the penguin loops have been neglected here. Thus the total weak phase $\phi_s^{SM}({\rm B_s^0} \to \phi\phi)$ is very close to zero. NP particles with extra CP phases can enter the decay ${\rm B_s^0} \to \phi\phi$ in mixing (box diagram) as well as in the penguin loop and affect the decay process. Therefore NP will change the mixing and decay phases $\Phi_{\rm M}({\rm B_s^0})$ and $\Phi_{\rm D}({\rm B_s^0} \to \phi\phi)$ and the total weak phase becomes

$$\begin{array}{ll} \phi_{\rm s}({\rm B_s^0} \to \phi\phi) & \equiv \phi_{\rm s}^{\rm SM}({\rm B_s^0} \to \phi\phi) + \Phi_{\rm M}^{\rm NP}({\rm B_s^0}) - \Phi_{\rm D}^{\rm NP}({\rm B_s^0} \to \phi\phi) \\ & = \phi_{\rm s}^{\rm SM}({\rm B_s^0} \to \phi\phi) + \phi_{\rm s}^{\rm NP}({\rm B_s^0} \to \phi\phi) \approx \phi_{\rm s}^{\rm NP}({\rm B_s^0} \to \phi\phi)\,. \end{array} \tag{10}$$

[1] LHCb will also be able to measure $\sin 2\beta^{eff}$ in the decay ${\rm B_d^0} \to \phi{\rm K_S^0}$ using the large sample of ${\rm B_d^0}$ events.

In general NP will affect B_s^0 mixing and the $b \to s$ penguin transition differently and we expect $\phi_s^{NP}(B_s^0 \to \phi\phi) = \Phi_D^{NP} - \Phi_D^{NP} \neq 0$. Thus any measurement of a non-zero CP asymmetry in $B_s^0 \to \phi\phi$ would imply new CP-violating phases in the penguin decay and/or B_s^0 mixing and be a clear NP signal. When combining with the decay $B_s^0 \to J/\psi\phi$ we will be able to disentangle new physics CP contributions in B_s^0 mixing and decay.

Table 1 Measurements and predictions for $\mathrm{BR}(B_s^0 \to \phi\phi)$. f_L and Γ_T/Γ is the fraction of longitudinal and transverse polarisation, respectively.

	BR[10^{-6}]	f_L	Γ_T/Γ [%]	Comments	Reference
Experiment	$14^{+6}_{-5}(\mathrm{stat.}) \pm 6(\mathrm{syst.})$	—	—		[4]
QCD Factorisation	$21.8^{+1.1+30.4}_{-1.1-17.0}$	43^{+0+61}_{-0-34}			[5]
	$19.5^{+1.0+13.1}_{-1.0-8.0}$	48^{+0+26}_{-0-27}		WA from data [a]	
QCD Factorisation	13.1		13.4	see erratum	[6]
Naive Factorisation	9.05		11.7	see erratum	
NLO EWP [a]	6.80		13.7	T and P [b]	[7]
	5.20		13.7	T, P and EWP [b]	
Factorization	0.37 — 25.1			Range	[8]

[a] WA stands for "Weak Annhilation".
[b] T, P and EWP stand for "Tree", "Penguin" and "Electroweak Penguin", respectively.

The branching ratio of the decay $B_s^0 \to \phi\phi$ has been measured to be

$$\mathrm{BR}(B_s^0 \to \phi\phi) = (14^{+6}_{-5}(\mathrm{stat.}) \pm 6(\mathrm{syst.})) \times 10^{-6} \tag{11}$$

by the CDF Collaboration [4]. The SM prediction of this branching ratio suffers from hadronic uncertainties. Results by various authors using different calculation methods are summarized in Table 1. We use the central value of the CDF branching ratio measurement for our estimate of the signal yield in LHCb, but vary it in the sensitivity study to see how it affects the statistical error of the ϕ_s measurement.

While many decay processes can be used to probe CP-violating new physics contributions to $b \to s$ penguin transitions, the process $B_s^0 \to \phi\phi$ has several experimental and theoretical features which make it a very interesting channel for the LHCb experiment.

- $B_s^0 \to \phi\phi$ followed by $\phi \to K^+K^-$ has only charged particles in the final state, which are easy to reconstruct experimentally;
- $B_s^0 \to \phi(K^+K^-)\phi(K^+K^-)$ has a relatively large visible branching ratio [10]

$$\begin{aligned} \mathrm{BR}^{\mathrm{vis}}(B_s^0 \to \phi(K^+K^-)\phi(K^+K^-)) &\equiv \mathrm{BR}(B_s^0 \to \phi\phi)\,[\mathrm{BR}(\phi \to K^+K^-)]^2 \\ &= (3.4 \pm 2.1) \times 10^{-6} \end{aligned} \tag{12}$$

  when compared with other $b \to s$ transitions. This advantage also compensates for the four times smaller fraction $f_s = 0.104$ for a $\overline{b}$ quark to hadronize into a B_s^0 meson compared to B_d^0 mesons.
- The LHCb RICH system provides good charged K/π separation to eliminate the large $\pi^\pm$ background;
- Measurements of the phases and the magnitudes of polarisation amplitudes in $B_s^0 \to \phi\phi$ provide insight into the chiral structure of b-quark flavour-changing neutral currents [5, 11, 12].

2 Monte Carlo Simulation

This study is based on Monte Carlo events generated using PYTHIA which have been fully simulated using GEANT4 programs in the LHCb Data Challenge 2004. In total 69 k $\mathrm{B_s^0} \to \phi\phi$ events are used for the signal study and approximately 34 million inclusive $\mathrm{b\bar{b}}$ events are used for the background study. The particles of interest, i.e. the signal-b hadron or one of the b-hadrons in the inclusive $\mathrm{b\bar{b}}$ events, are required to have a true polar angle smaller than 400 mrad. The sizes of the data samples mentioned above are given after this requirement. The efficiency of this angular acceptance is $\varepsilon_\theta^{\mathrm{s}}$ = 34.7% for signal B events and $\varepsilon_\theta^{\mathrm{b}}$ = 43.4% for inclusive $\mathrm{b\bar{b}}$ events.

3 $\mathrm{B_s^0} \to \phi\phi$ Selection

3.1 Preselection

An event preselection procedure was used as a first step in order to suppress most of the 34 million inclusive $\mathrm{b\bar{b}}$ events. This was carried out by employing kinematic and topological criteria. The preselection is performed by

- Requiring the impact parameter significance of charged kaon candidates with regard to all primary vertices to be greater than 2;
- Requiring the difference of log-likelihood values between the kaon hypothesis and the pion hypothesis to be larger than -2 for all charged kaon candidates;
- Requiring the invariant mass of the ϕ candidates to be lower than 1050 MeV/c^2;
- Requiring the χ^2 of the ϕ vertices to be smaller than 100;
- Requiring the χ^2 of the $\mathrm{B_s^0}$ vertices to be smaller than 36;
- Requiring the invariant mass of the $\mathrm{B_s^0}$ candidates to be within the range (4 $\mathrm{GeV/c^2}$, 7 $\mathrm{GeV/c^2}$).

This preselection reduces the amount of inclusive $\mathrm{b\bar{b}}$ events by a factor of 2100. In total 15839 events are preselected from the 34 million inclusive $\mathrm{b\bar{b}}$ events. 5843 events are preselected from the 69 k signal events, of which only 8768 have all the four kaons reconstructed.

3.2 Selection Criteria

Using the events that passed the preselection we developed criteria to select efficiently the signal events while rejecting all the background available for this analysis. This is necessary since the 34 million inclusive $\mathrm{b\bar{b}}$ events corresponds to 13 minutes of data taking only, whereas the signal sample is equivalent to 4.8×10^4 minutes (33 days) of data taking. No optimisation procedure has been used to define the selection cuts.

As the signal and background samples correspond to different data taking time periods, all the background and signal distributions shown in this section are normalized to the same area for better clarity.

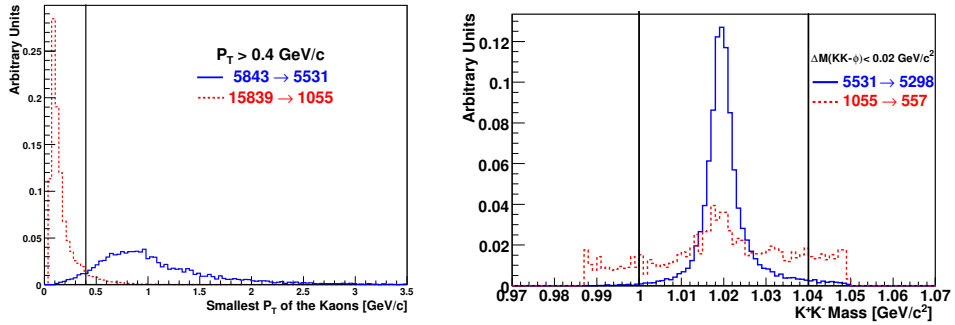

Figure 2 On the left we show the smallest $\mathrm{P_T}$ of the kaons and on the right the mass of the ϕ candidates. The signal and inclusive $\mathrm{b\overline{b}}$ distributions are represented by the solid and dashed histograms, respectively. The applied cuts are indicated by the vertical lines. Also shown is the reduction in number of events produced by the cuts.

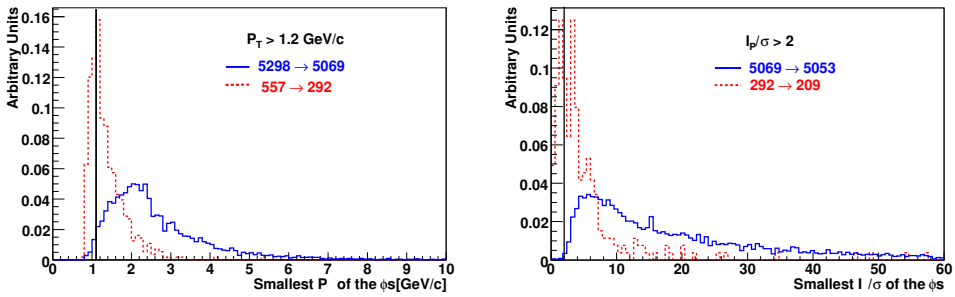

Figure 3 On the left we show the smallest $\mathrm{P_T}$ and on the right the smallest impact parameter significance of the ϕ candidates. The signal and inclusive $\mathrm{b\overline{b}}$ distributions are represented by the solid and dashed histograms, respectively. The applied cuts are indicated by the vertical lines. Also shown is the reduction in number of events produced by the cuts.

In Fig. 2 (left) we show distributions of the smallest transverse momenta $\mathrm{P_T}$ of the kaons both for the signal and the inclusive $\mathrm{b\overline{b}}$ data samples. We require the kaons to satisfy $\mathrm{P_T} > 400\,\mathrm{MeV}/c$.

The distributions of the reconstructed mass M_ϕ of the ϕ candidates are shown for both the signal and inclusive $\mathrm{b\overline{b}}$ samples in Fig. 2 (right). A mass window of $\Delta M_\phi = \pm\ 20\ \mathrm{MeV}/c^2$ around $1019.5\ \mathrm{MeV}/c^2$ is applied and indicated in the plot.

The distributions of the smallest $\mathrm{P_T}$ of the ϕ candidates are shown in Fig. 3 (left). We require $\mathrm{P_T} > 1.2\,\mathrm{GeV}/c$ for all ϕ candidates.

The distributions of the smallest impact parameter siginificance IP/σ of the ϕ particles with regard to primary vertices in signal and inclusive $\mathrm{b\overline{b}}$ events are shown in Fig. 3 (right). We require $\mathrm{IP}/\sigma > 2$ for all ϕ candidates.

The distributions of $\mathrm{B_s^0}$ vertex $\chi^2(\mathrm{B_s^0})$ for both signal and $\mathrm{b\overline{b}}$ events are shown in Fig. 4 (left). We require $\chi^2(\mathrm{B_s^0}) < 25$.

The distributions of the difference along the z axis $\mathrm{D_Z}(\mathrm{B_s^0})$ between the $\mathrm{B_s^0}$ decay vertex and the primary vertex are shown for both signal and $\mathrm{b\overline{b}}$ events in Fig. 4 (right). We require $\mathrm{D_Z}(\mathrm{B_s^0})$ to be positive.

The mass window for signal counting is chosen to be $\Delta\mathrm{M}(\mathrm{B_s^0}) = \pm 40\ \mathrm{MeV}/c^2$. This is based on the $\mathrm{B_s^0}$ mass resolution obtained from a Gaussian fit to the signal mass distribution shown in

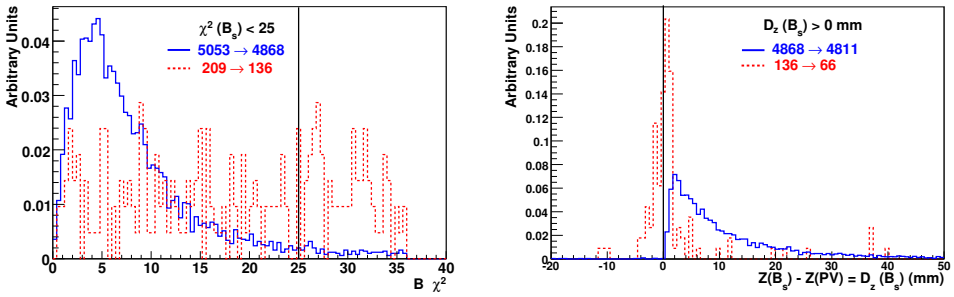

Figure 4 On the left we show the χ^2 distribution of the $\mathrm{B_s^0}$ vertex and on the right the distribution of the signed z distance between the $\mathrm{B_s^0}$ decay vertex and the primary vertex. The signal and inclusive $\mathrm{b\overline{b}}$ distributions are represented by the solid and dashed histograms, respectively. The applied cuts are indicated by the vertical lines. Also shown is the reduction in number of events produced by the cuts.

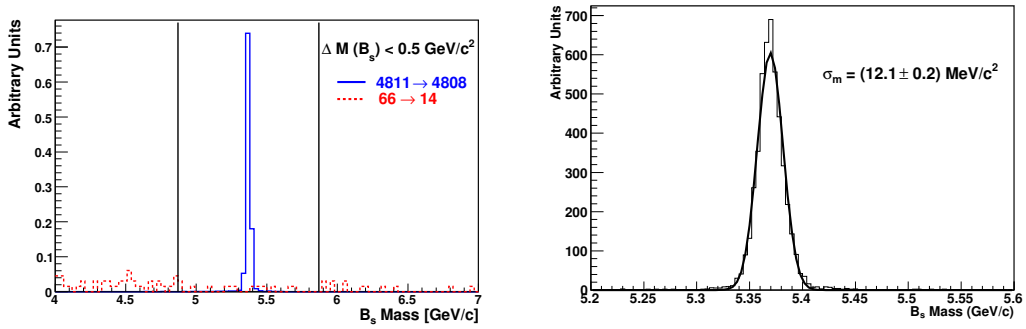

Figure 5 On the left we show the $\mathrm{B_s^0}$ mass spectrum. The signal and inclusive $\mathrm{b\overline{b}}$ distributions are represented by the solid and dashed histograms, respectively. The applied cuts are indicated by the vertical lines. Also shown is the reduction in number of events produced by the cuts. On the right we show the accepted events inside the broader mass window together with a Gaussian fit to obtain the mass resolution σ_m.

Fig. 5.

In order to increase statistics for the background estimation, a broader mass window is used for the background data sample. We require $\Delta\mathrm{M}(\mathrm{B_s^0}) \pm 500\,\mathrm{MeV}/c^2$ (see Fig. 5). Assuming the background events are evenly distributed in this mass window, counting $\mathrm{b\overline{b}}$ events in the broader window is equivalent to increasing the $\mathrm{b\overline{b}}$ sample by a factor of 12.5.

The offline selection is summarized in Table 2.

3.3 Trigger and Tagging Performances

The trigger and tagging [9] algorithms are run on the offline selected events and the results are shown in Table 3. Notice the signal events are counted inside the tighter mass window and the inclusive $\mathrm{b\overline{b}}$ in the the broader mass window. We can see that no background event passes both offline selection and trigger. For completeness we describe the higher level trigger for this channel in Appendix A.

Table 2 Summary of the applied cuts in the offline selection and the amount of events left after each cut is applied.

	Number of Events	
Applied Cut	Signal Sample	Background Sample
Generated	69000	33926781
Preselection	5843	15839
$\mathrm{P_T(K)} > 400$ MeV/c	5531	1055
$\Delta\mathrm{M}(\phi) < 20$ MeV/c^2	5298	557
$\mathrm{P_T}(\phi) > 1200$ MeV/c	5069	292
$\mathrm{IP}/\sigma(\phi) > 2$	5053	209
$\chi^2(\mathrm{B_s^0}) < 25$	4868	136
$\mathrm{D_Z}(\mathrm{B_s^0}) > 0$ mm	4811	66
$\Delta\mathrm{M}(\mathrm{B_s^0}) < 500$ MeV/c^2	-	14
$\Delta\mathrm{M}(\mathrm{B_s^0}) < 40$ MeV/c^2	4663	-

Table 3 Result of the trigger and tagging algorithms in the events accepted by the offline selection. The analysis is sequential in a such way that only events accepted by the previous level are considered by the next one. Note that the mass windows used for the signal and background selections are different.

	Number of Events	
Selection	Signal	Inclusive $\mathrm{b\bar{b}}$
Offline	4663	14
L0	1716 ($\epsilon_{\mathrm{L0}} = 0.368 \pm 0.007$)	5
L1	1208 ($\epsilon_{\mathrm{L1}} = 0.704 \pm 0.011$)	4
HLT	870 ($\epsilon_{\mathrm{HLT}} = 0.720 \pm 0.013$)	0
Tagging	592 ($\epsilon_{\mathrm{tag}} = 0.680 \pm 0.016$)	0

3.4 Event Yields

The expected number of signal events in a nominal year is given by

$$\mathrm{N_{sig}} = \mathcal{L}_{\mathrm{int}} \times \sigma_{\mathrm{b\bar{b}}} \times 2 \times \mathrm{f_s} \times \mathrm{BR^{vis}}(\mathrm{B_s^0} \to \phi(\mathrm{K^+K^-})\phi(\mathrm{K^+K^-})) \times \epsilon_{\mathrm{sig}}^{\mathrm{tot}} \tag{13}$$

where $\mathcal{L}_{\mathrm{int}} = 2\ \mathrm{fb}^{-1}$ is the integrated luminosity in 10^7 s of data taking and $\sigma_{\mathrm{b\bar{b}}} = 500\mu\mathrm{b}$ is the $\mathrm{b\bar{b}}$ production cross section in proton-proton collisions at 14 TeV. The product $\mathcal{L}_{\mathrm{int}} \times \sigma_{\mathrm{b\bar{b}}} \approx 1.0 \times 10^{12}$ is the expected number of $\mathrm{b\bar{b}}$ pairs produced in a $2\ \mathrm{fb}^{-1}$ data sample. The fraction $\mathrm{f_s} = 0.104$ is the probability of a $\bar{\mathrm{b}}$ quark to hadronize into a $\mathrm{B_s^0}$ meson [10] and the factor 2 is due to the fact that there are always both a b and a $\bar{\mathrm{b}}$ produced in an event. The visible branching ratio $\mathrm{BR^{vis}}(\mathrm{B_s^0} \to \phi(\mathrm{K^+K^-})\phi(\mathrm{K^+K^-})) = (3.4 \pm 2.1) \times 10^{-6}$ is given in Equ. 12 and ϵ_{sig}^{tot} is the total signal efficiency:

$$\epsilon_{\mathrm{sig}}^{\mathrm{tot}} = \varepsilon_\theta^{\mathrm{s}} \times \epsilon_{\mathrm{sig}}^{\mathrm{sel}} \tag{14}$$

where $\varepsilon_\theta^{\mathrm{s}} = 0.347$ is the geometrical acceptance for the signal sample, $\epsilon_{\mathrm{sig}}^{\mathrm{sel}}$ is the total efficiency for the signal events inside the geometrical acceptance to pass the trigger, reconstruction and offline selections. Since 870 signal events out of the 69000 signal events generated inside the acceptance have passed all the trigger and offline selection cuts, we obtain

$$\epsilon_{\mathrm{sig}}^{\mathrm{sel}} = 870/69000 = 1.26 \times 10^{-2}. \tag{15}$$

The expected number of triggered and selected $\mathrm{B_s^0} \to \phi\phi$ events in $2\ \mathrm{fb}^{-1}$ of data is:

$$\mathrm{N_{sig}} = 3092 \pm 105, \tag{16}$$

where the error is statistical only. Among them 2096 ± 86 events will be flavour tagged with a mistag rate of about 0.3.

The expected number of background events in a nominal year estimated with the inclusive $\mathrm{b\overline{b}}$ events is given by

$$\mathrm{N_{b\bar{b}}} = \mathcal{L}_{\mathrm{int}} \times \sigma_{\mathrm{b\bar{b}}} \times \epsilon_{\mathrm{b\overline{b}}}^{\mathrm{tot}} \tag{17}$$

where the integrated luminosity and the cross section of $\mathrm{b\bar{b}}$ pairs are the same as mentioned above. The total efficiency for selecting background $\epsilon_{\mathrm{b\bar{b}}}$ is

$$\epsilon_{\mathrm{b\overline{b}}}^{\mathrm{tot}} = \varepsilon_\theta^{\mathrm{b}} \times \epsilon_{\mathrm{b\overline{b}}}^{\mathrm{mass}} \times \epsilon_{\mathrm{b\overline{b}}}^{\mathrm{sel}} \tag{18}$$

where $\varepsilon_\theta^{\mathrm{b}} = 0.434$ is the geometrical acceptance for the inclusive $\mathrm{b\overline{b}}$ sample, and $\epsilon_{\mathrm{b\overline{b}}}^{\mathrm{mass}}$ is due to the difference in the mass windows used for the signal and background selection. This is defined as the ratio of the sizes of the signal mass window to that of the background mass window: $\epsilon_{\mathrm{b\overline{b}}}^{\mathrm{mass}} = 40/500 = 0.08$. The total efficiency for the $\mathrm{b\overline{b}}$ events inside the geometrical acceptance to pass the trigger, reconstruction and offline selections is $\epsilon_{\mathrm{b\overline{b}}}^{\mathrm{sel}}$. Since no $\mathrm{b\overline{b}}$ events are selected, the upper limit of $\epsilon_{\mathrm{b\overline{b}}}^{\mathrm{sel}}$ at 90% confidence level (CL) following Poisson statistics is

$$\epsilon_{\mathrm{b\overline{b}}}^{\mathrm{sel}} = 2.3/(33.9 \times 10^6) = 6.8 \times 10^{-8} \tag{19}$$

where 33.9×10^6 is the number of $\mathrm{b\overline{b}}$ events used in the study. This leads to a total yield of

$$\mathrm{N_{b\overline{b}}} < 2.4 \times 10^3 \tag{20}$$

at 90% CL for a $2\ \mathrm{fb}^{-1}$ data sample. The obtained numbers of signal and background events can be translated into an upper limit on the background to signal ratio,

$$\mathrm{B/S} < 0.8 \tag{21}$$

at 90 % CL.

The background to signal ratio estimated without applying trigger is $\mathrm{B/S} = 0.86 \pm 0.23$.

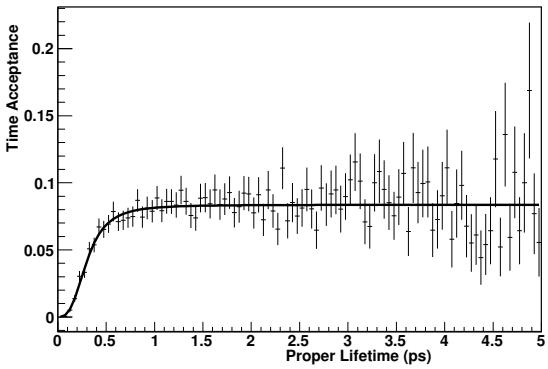

Figure 6 Ratio of the histograms with the proper time between the offline selected events and the generated ones. The fit is the function $\epsilon^{\mathrm{A}}(\mathrm{t}) = \frac{\mathrm{at}^3}{\mathrm{b}+\mathrm{t}^3}$.

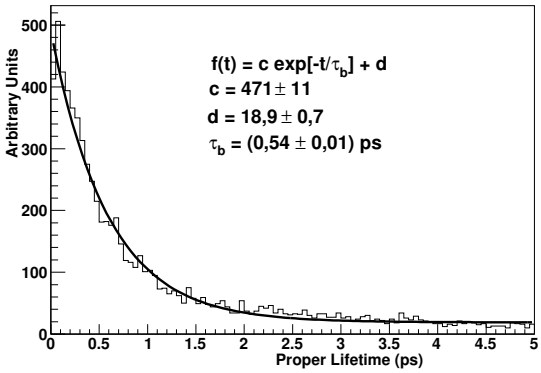

Figure 7 Distribution of measured proper time of preselected $\mathrm{b\overline{b}}$ events. A fit of the function $\mathrm{f(t)} = \mathrm{ce}^{-\mathrm{t}/\tau_\mathrm{b}} + \mathrm{d}$ is performed.

3.5 Proper Time Acceptance Function

In order to obtain the time acceptance function $\epsilon^{\mathrm{A}}(\mathrm{t})$ that gives the efficiency of measuring a given proper time t, we plot the ratio of the the histogram of the measured t for the offline selected events to the histogram of all generated t values in Fig. 6. A fit of the function

$$\epsilon^{\mathrm{A}}(\mathrm{t}) = \frac{\mathrm{at}^3}{\mathrm{b} + \mathrm{t}^3} \tag{22}$$

to the ratio histogram gives a = 0.084 $\pm$ 0.001 and b = (0.027 $\pm$ 0.003) ps^3.

Because of the stripping, we only have access to the preselected background events, therefore we use the preselected events to estimate the mean lifetime of background events. We fit a function of the form $\mathrm{f(t)} = \mathrm{c} \times \mathrm{e}^{-\mathrm{t}/\tau_\mathrm{b}} + \mathrm{d}$ to the proper time distribution of all preselected $\mathrm{b\overline{b}}$ events and obtain $\tau_b = (0.54 \pm 0.01)$ ps (Fig. 7). The fit shows that the inclusive $\mathrm{b\overline{b}}$ events have an exponential proper time spectrum with τ_b as its mean lifetime.

A fit of the function $\mathrm{h(t)} = \epsilon^{\mathrm{A}}(\mathrm{t}) \times \mathrm{e}^{-\mathrm{t}/\tau_\mathrm{b}}$ to the offline accepted $\mathrm{b\overline{b}}$ events gives $\mathrm{a} = 10 \pm 16$ and $\mathrm{b} = (1.2 \pm 0.7) \times 10^{-4}$ ps^3.

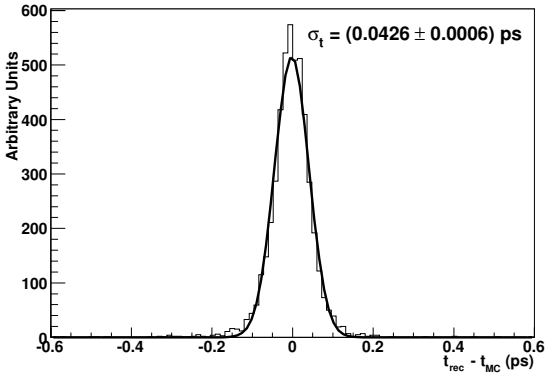

Figure 8 Difference between the measured and the generated proper time in signal events accepted by the offline and trigger selection. Also shown is a Gaussian fit that gives a resolution of $\sigma_{\rm t} = 0.0426$ ps.

3.6 Proper Time Resolution

The distribution of the difference between the measured and the generated proper time of the signal events passing offline selection and trigger is shown in Fig. 8. A Gaussian fit to the distribution gives $\sigma_{\rm t} = (42.6 \pm 0.6)$ fs.

4 Sensitivity Study

4.1 Time-dependent Angular Distribution

For decays of $\rm B_s^0$ to a CP eigenstate f, new physics can manifest itself in CP violation in the inteference between decays with and without mixing, which can be probed by measuring the time-dependent CP asymmetry

$$\mathcal{A}(t) \equiv \frac{\Gamma\left[\overline{\rm B}_{\rm s}^0({\rm t}) \to {\rm f}\right] - \Gamma\left[{\rm B}_{\rm s}^0({\rm t}) \to {\rm f}\right]}{\Gamma\left[\overline{\rm B}_{\rm s}^0({\rm t}) \to {\rm f}\right] + \Gamma\left[{\rm B}_{\rm s}^0({\rm t}) \to {\rm f}\right]} = \frac{\mathcal{A}^{\rm dir}{\rm cos}(\Delta {\rm m_s t}) + \mathcal{A}^{\rm mix}{\rm sin}(\Delta {\rm m_s t})}{{\rm cosh}(\Delta\Gamma_{\rm s}{\rm t}/2) - \mathcal{A}^{\Delta\Gamma}{\rm sinh}(\Delta\Gamma_{\rm s}{\rm t}/2)}, \tag{23}$$

where $\Delta m_{\rm s}$ and $\Delta\Gamma_{\rm s}$ are the mass and width difference between the heavy and light $\rm B_s^0$ mesons mass eigenstates

$$\Delta {\rm m_s} = {\rm M_H} - {\rm M_L}, \quad \Delta\Gamma_{\rm s} = \Gamma_{\rm L} - \Gamma_{\rm H}\ . \tag{24}$$

The CP asymmetries $\mathcal{A}^{\rm dir}$, $\mathcal{A}^{\rm mix}$ and $\mathcal{A}^{\Delta\Gamma}$ are

$$\mathcal{A}^{\rm dir} = \frac{|\lambda_{\rm f}|^2 - 1}{1 + |\lambda_{\rm f}|^2}, \tag{25}$$

$$\mathcal{A}^{\rm mix} = \frac{2\mathcal{I}{\rm m}\lambda_{\rm f}}{1 + |\lambda_{\rm f}|^2} \tag{26}$$

and

$$\mathcal{A}^{\Delta\Gamma} = \frac{2\mathcal{R}{\rm e}\lambda_{\rm f}}{1 + |\lambda_{\rm f}|^2}\ . \tag{27}$$

The quantity λ_f is given by

$$\lambda_{\rm f} = \frac{\rm q}{\rm p}\frac{\bar{\rm A}_{\rm f}}{\rm A_f} = \eta_{\rm f}\frac{\rm q}{\rm p}\frac{\bar{\rm A}_{\bar{\rm f}}}{\rm A_f} \tag{28}$$

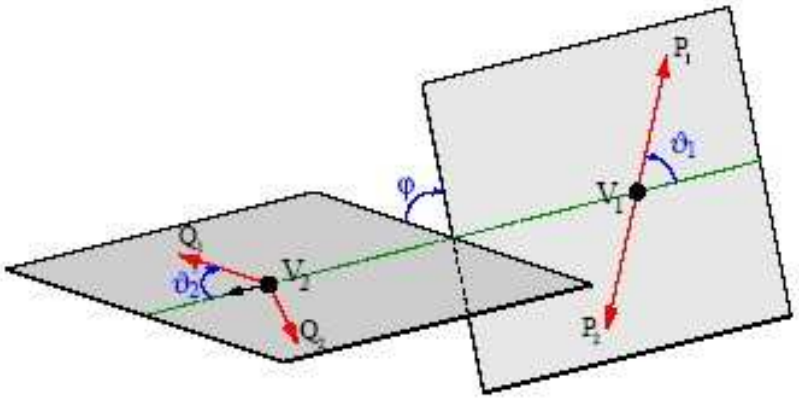

Figure 9 Definitions of the decay angles θ_1, θ_2 and φ for a general $B \to V_1 V_2$ decay, taken from Ref. [5]. In this note we identify $\mathrm{B_s^0} \to \phi(\mathrm{K^+K^-})\phi(\mathrm{K^+K^-})$ with $B \to V_1(P_1P_2)V_2(Q_1Q_2)$.

.

where $\eta_f = \pm 1$ is the CP eigenvalue of the final state f. The quantities $\mathcal{A}^{\rm dir}$, $\mathcal{A}^{\rm mix}$ and $\mathcal{A}^{\Delta\Gamma}$ are not independent but fulfill the relation

$$|\mathcal{A}^{\rm dir}|^2 + |\mathcal{A}^{\rm mix}|^2 + |\mathcal{A}^{\Delta\Gamma}|^2 \equiv 1. \tag{29}$$

In the case of $\mathrm{B_s^0} \to \phi\phi$, the final state is an admixture of CP even and CP odd eigenstates, just like in $\mathrm{B_s^0} \to \mathrm{J/}\psi\phi$. An angular analysis of the decay products $\mathrm{B_s^0} \to \phi(\mathrm{K^+K^-})\phi(\mathrm{K^+K^-})$ is required to disentangle the different CP components. A special feature of $\mathrm{B_s^0} \to \phi\phi$ compared to $\mathrm{B_s^0} \to \mathrm{J/}\psi\phi$ is that the two ϕ particles are identical so that we need to choose a basis in which the two $\mathrm{K^+K^-}$ pairs from the two ϕ's are treated symmetrically in order to obey Bose statistics.

For a $\mathrm{B_s^0}$ meson at $t = 0$, the time dependent angular distribution of the decay chain $\mathrm{B_s^0} \to \phi(\mathrm{K^+K^-})\phi(\mathrm{K^+K^-})$ can be written as

$$\frac{\mathrm{d}\Gamma(\mathrm{t})}{\mathrm{d}\cos\theta_1 \mathrm{d}\cos\theta_2 \mathrm{d}\varphi_1 \mathrm{d}\varphi_2} \propto \left| \sum_{\mathrm{h}=0,\pm 1} \mathrm{H_h(t)} \mathrm{D^{1*}_{h,0}}(\varphi_1, \theta_1, 0) \mathrm{D^{1*}_{h,0}}(\varphi_2, \theta_2, 0) \right|^2 \tag{30}$$

where $\mathrm{h} = 0, \pm 1$ denotes the ϕ_1 helicity, which is equal to the ϕ_2 helicity, $H_{\rm h}(t)$ is the time-dependent helicity amplitude and the D-function is defined as $D^j_{mn}(\alpha, \beta, \gamma) = e^{-im\alpha} d^j_{mn}(\beta) e^{-in\gamma}$. As shown in Fig. 9 we define $\theta_1(\theta_2)$ and $\varphi_1(\varphi_2)$ as the polar and azimuthal angles of the $\mathrm{K^+}_1$($\mathrm{K^+}_2$) momentum in the rest frame of their mother $\phi_1(\phi_2)$. The convention used is as follows: the $z'(z'')$ axis is defined as the direction of the $\phi_1(\phi_2)$ momentum in the rest frame of the $\mathrm{B_s^0}$; the $x'(x'')$ axis is an arbitrarily chosen direction in the plane normal to the $z'(z'')$ axis and the x' and x'' axes are defined to be opposite to each other; then the y' and y'' axes are fixed uniquely. The angle between the decay planes of the two ϕ's is given by

$$\varphi \equiv \varphi_1 + \varphi_2, \tag{31}$$

and we integrate out $\varphi_1 - \varphi_2$.

We replace the helicity amplitudes $\mathrm{H_{0,\pm 1}(t)}$ with the linear polarisation amplitudes $\mathrm{A_{0,\|,\perp}(t)}$ in the transversity basis

$$
\begin{aligned}
\mathrm{A}_0(\mathrm{t}) &\equiv \mathrm{H}_0(\mathrm{t}), \\
\mathrm{A}_{\parallel}(\mathrm{t}) &\equiv (\mathrm{H}_{+1}(\mathrm{t}) + \mathrm{H}_{-1}(\mathrm{t}))/\sqrt{2}, \\
\mathrm{A}_{\perp}(\mathrm{t}) &\equiv (\mathrm{H}_{+1}(\mathrm{t}) - \mathrm{H}_{-1}(\mathrm{t}))/\sqrt{2}.
\end{aligned}
\tag{32}
$$

We obtain for the differential decay distribution

$$
\frac{\mathrm{d}\Gamma(\mathrm{t})}{\mathrm{dcos}\theta_1 \mathrm{dcos}\theta_2 \mathrm{d}\varphi} \propto \sum_{\mathrm{j}=0}^{6} \mathrm{K_j(t) f_j}(\theta_1, \theta_2, \varphi). \tag{33}
$$

The angular functions $f_j(\theta_1, \theta_2, \varphi)$ of Equ. 33 are given by

$$
\begin{aligned}
\mathrm{f}_1(\theta_1, \theta_2, \varphi) &= 4\mathrm{cos}^2\theta_1 \mathrm{cos}^2\theta_2, \\
\mathrm{f}_2(\theta_1, \theta_2, \varphi) &= \mathrm{sin}^2\theta_1 \mathrm{sin}^2\theta_2 (1 + \mathrm{cos}2\varphi), \\
\mathrm{f}_3(\theta_1, \theta_2, \varphi) &= \mathrm{sin}^2\theta_1 \mathrm{sin}^2\theta_2 (1 - \mathrm{cos}2\varphi), \\
\mathrm{f}_4(\theta_1, \theta_2, \varphi) &= -2\mathrm{sin}^2\theta_1 \mathrm{sin}^2\theta_2 \mathrm{sin}2\varphi, \\
\mathrm{f}_5(\theta_1, \theta_2, \varphi) &= \sqrt{2}\mathrm{sin}2\theta_1 \mathrm{sin}2\theta_2 \mathrm{cos}\varphi, \\
\mathrm{f}_6(\theta_1, \theta_2, \varphi) &= -\sqrt{2}\mathrm{sin}2\theta_1 \mathrm{sin}2\theta_2 \mathrm{sin}\varphi.
\end{aligned}
\tag{34}
$$

The time-dependent functions $K_j(t)$ of Equ. 33 are defined as

$$
\begin{aligned}
\mathrm{K}_1(\mathrm{t}) &= |\mathrm{A}_0(\mathrm{t})|^2, \\
\mathrm{K}_2(\mathrm{t}) &= \left|\mathrm{A}_{\parallel}(\mathrm{t})\right|^2, \\
\mathrm{K}_3(\mathrm{t}) &= |\mathrm{A}_{\perp}(\mathrm{t})|^2, \\
\mathrm{K}_4(\mathrm{t}) &= \mathcal{I}\mathrm{m}(\mathrm{A}^*_{\parallel}(\mathrm{t})\mathrm{A}_{\perp}(\mathrm{t})), \\
\mathrm{K}_5(\mathrm{t}) &= \mathcal{R}\mathrm{e}(\mathrm{A}^*_0(\mathrm{t})\mathrm{A}_{\parallel}(\mathrm{t})), \\
\mathrm{K}_6(\mathrm{t}) &= \mathcal{I}\mathrm{m}(\mathrm{A}^*_0(\mathrm{t})\mathrm{A}_{\perp}(\mathrm{t})).
\end{aligned}
\tag{35}
$$

The most general form of the $\mathrm{K_j(t)}$ functions requires different λ_f terms for different polarisation and thus the functions become complicated. In the SM all the three polarisation states can be very well parameterised using one common complex factor λ_f. Then the $\mathrm{K_j(t)}$ functions can

be written as

$$
\begin{aligned}
\mathrm{K_1(t)} = \;& \tfrac{1}{2}\mathrm{A_0^2}\left[(1+\cos\phi_s)\mathrm{e}^{-\Gamma_L t}+(1-\cos\phi_s)\mathrm{e}^{-\Gamma_H t}+2\mathrm{e}^{-\Gamma_s t}\sin(\Delta m_s t)\sin\phi_s\right],\\
\mathrm{K_2(t)} = \;& \tfrac{1}{2}\mathrm{A_{\|}^2}\left[(1+\cos\phi_s)\mathrm{e}^{-\Gamma_L t}+(1-\cos\phi_s)\mathrm{e}^{-\Gamma_H t}+2\mathrm{e}^{-\Gamma_s t}\sin(\Delta m_s t)\sin\phi_s\right],\\
\mathrm{K_3(t)} = \;& \tfrac{1}{2}\mathrm{A_{\perp}^2}\left[(1-\cos\phi_s)\mathrm{e}^{-\Gamma_L t}+(1+\cos\phi_s)\mathrm{e}^{-\Gamma_H t}-2\mathrm{e}^{-\Gamma_s t}\sin(\Delta m_s t)\sin\phi_s\right],\\
\mathrm{K_4(t)} = \;& |\mathrm{A_{\|}}||\mathrm{A_{\perp}}|[\mathrm{e}^{-\Gamma_s t}\{\sin\delta_1\cos(\Delta m_s t)-\cos\delta_1\sin(\Delta m_s t)\cos\phi_s\}\\
& -\tfrac{1}{2}\left(\mathrm{e}^{-\Gamma_H t}-\mathrm{e}^{-\Gamma_L t}\right)\cos\delta_1\sin\phi_s], \qquad (36)\\
\mathrm{K_5(t)} = \;& \tfrac{1}{2}|\mathrm{A_0}||\mathrm{A_{\|}}|\cos(\delta_2-\delta_1)\\
& \left[(1+\cos\phi_s)\mathrm{e}^{-\Gamma_L t}+(1-\cos\phi_s)\mathrm{e}^{-\Gamma_H t}+2\mathrm{e}^{-\Gamma_s t}\sin(\Delta m_s t)\sin\phi_s\right],\\
\mathrm{K_6(t)} = \;& |\mathrm{A_0}||\mathrm{A_{\perp}}|[\mathrm{e}^{-\Gamma_s t}\{\sin\delta_2\cos(\Delta m_s t)-\cos\delta_2\sin(\Delta m_s t)\cos\phi_s\}\\
& -\tfrac{1}{2}\left(\mathrm{e}^{-\Gamma_H t}-\mathrm{e}^{-\Gamma_L t}\right)\cos\delta_2\sin\phi_s]
\end{aligned}
$$

where $\phi_s = \phi_s(\mathrm{B_s^0}\to\phi\phi)$ is the total weak phase. The strong phases δ_1 and δ_2 are predicted by QCD factorisation to be [13]:

$$
\begin{aligned}
\delta_1 &\equiv \arg(\mathrm{A_{\perp}}/\mathrm{A_{\|}}) = 0\ ,\\
\delta_2 &\equiv \arg(\mathrm{A_{\perp}}/\mathrm{A_0}) = \pi\ .
\end{aligned} \qquad (37)
$$

These values are used for the purpose of simulating the sensitivity. But we will determine these phases from the angular analysis and not rely on the QCD factorisation values. The normalisation condition is $|\mathrm{A_0}|^2+|\mathrm{A_{\|}}|^2+|\mathrm{A_{\perp}}|^2=1$.

The time-dependent angular distribution for a $\overline{\mathrm{B}}{}_s^0$ meson at $t=0$ can be obtained by reversing the sign of the terms proportional to $\sin(\Delta m_s)$ or $\cos(\Delta m_s)$ in the $\mathrm{K_j(t)}$ functions.

4.2 New Physics Search Strategy

We aim for a null test of the SM instead of measurements of the magnitudes and phases of the NP contributions to the decay amplitudes, which can only be done in some specific models with certain constraints to relate the NP magnitudes and phases, because in general the number of unknowns exceeds the number of observables [14].

A general way of testing the SM using $\mathrm{B_s^0}\to\phi\phi$ is to measure $\mathcal{A}_l^{\mathrm{dir}}$, $\mathcal{A}_l^{\mathrm{mix}}$ and $\mathcal{A}_l^{\Delta\Gamma}$ for each linear polarisation $l = 0$, $\|$ or $\perp$ without using any parameterization of NP [2]. These quantities

[2] In Ref.[14] 18 physical observables can be extracted from the time dependent decay rates. The CP asymmetries are the most interesting ones.

can be directly compared with their SM predictions

$$\mathcal{A}_{\rm l}^{\rm dir,SM} \cong 0,$$

$$\mathcal{A}_{\rm l}^{\rm mix,SM} = \eta_{\rm l}\sin(\phi_{\rm s}^{\rm SM}) \cong 0, \tag{38}$$

$$\mathcal{A}_{\rm l}^{\Delta\Gamma,\rm SM} = \cos(\phi_{\rm s}^{\rm SM}) \cong 1.$$

These model-independent observables also provide the possibility to obtain or constrain NP model parameters in different models without re-analyses of the experimental data. This method will be a natural choice for the exploitation of the real data. But in this study a different and intuitive method is used to avoid the inconvenience of quoting experimental errors and covariances for the nine CP asymmetries in Equ. 38, out of which six are independent.

Unlike the SM case, in principle $\phi_{\rm s}$ can be different for the three polarisation states when NP is concerned [15, 14]. We simply assume that the SM is valid so that $\phi_{\rm s}$ is polarisation independent

$$\phi_{\rm s}(0) = \phi_{\rm s}(\|) = \phi_{\rm s}(\perp) \tag{39}$$

and look for a deviation of $\phi_{\rm s}$ from its SM prediction.

As pointed out in [14, 15], the relation (39) can be violated if SM contributions and NP contributions to the decay amplitudes have different strong phases due to final state rescattering. This means we should check the consistency of the assumption (39) with data when we use it to measure a unique total weak phase.

The method for a null test of the SM consists of three steps:

1. perform a unbinned maximum likelihood fit to determine the total weak phase $\phi_{\rm s}$;
2. perform a goodness-of-fit test to see if the likelihood function based on Equ. 39 is consistent with data or not;
3. compare the measured $\phi_{\rm s}$with its SM prediction.

If the goodness-of-fit test fails, the SM is not necessarily rejected unless other possibility of wrong modelling is excluded. In the inconclusive case we need to use the general method described at the beginning of 4.2. To obtain the goodness-of-fit after the unbinned maximum likelihood fit, we can simply bin the data and construct a χ^2 statistic for Poisson distributed data. The χ^2 value is a measure of consistency between the used model and data.

If the goodness-of-fit test is passed, then we can proceed to the null test of the SM using $\phi_{\rm s}$ as a test statistic. The null hypothesis is $\phi_{\rm s} = 0$. Failing this test implies NP with new CP phases.

4.3 Fast Monte Carlo Simulations

We perform a fast Monte Carlo simulation to estimate the statistical error of the measurement of the total weak phase $\phi_{\rm s}$ using as input the signal yield, B/S, proper time acceptance functions and resolutions from the full simulation described in Section 3. This is done in the following steps :

- describe the distribution of the decay variables with a probability density function (PDF);

- generate Monte Carlo events according to this PDF;
- fit a PDF with the same form but free parameters to the generated data;
- repeat the above two steps (called an experiment) large number of times;
- estimate statistical errors of the fit parameters from the distributions of the differences between the input values and the fitted values.

The total PDF $\mathrm{p_{tot}}$ for all distributions can be written as

$$\mathrm{p_{tot}} = (1 - \mathrm{f_b})\mathrm{p_{sig}} + \mathrm{f_b}\mathrm{p_{bg}} \tag{40}$$

where $\mathrm{p_{sig}}$ denotes the total signal PDF, $\mathrm{p_{bg}}$ denotes the total background PDF and $\mathrm{f_b}$ denotes the fraction of background events in the event sample.

Both the signal PDF and the background PDF have the form

$$\mathrm{p_{sig(bg)}} = \epsilon^{\mathrm{A}}_{\mathrm{sign(bg)}}(\mathrm{t}) \times \mathrm{p}^{\mathrm{4D}}_{\mathrm{sig(bg)}}(\mathrm{t}, \cos\theta_1, \cos\theta_2, \varphi, \mathrm{I_{cat}}) \times \mathrm{p}^{\mathrm{mass}}_{\mathrm{sig(bg)}}(\mathrm{m_{B^0_s}}), \tag{41}$$

where $\epsilon^{\mathrm{A}}(\mathrm{t})$ is the efficiency as a function of the reconstructed proper time (usually called proper time acceptance function), $\mathrm{I_{cat}}$ denotes tagged $\mathrm{B^0_s}$-flavour which can take values +1, 0, -1 (corresponding to tagged as $\mathrm{B^0_s}$, untagged, tagged as $\overline{\mathrm{B}}^0_\mathrm{s}$), $\mathrm{p}^{\mathrm{4D}}(\mathrm{t}, \cos\theta_1, \cos\theta_2, \varphi, \mathrm{I_{cat}})$ is the time-dependent angular distribution and $\mathrm{p}^{\mathrm{mass}}(\mathrm{m_{B^0_s}})$ is the distribution of the reconstructed $\mathrm{B^0_s}$ mass, denoted as $\mathrm{m_{B^0_s}}$.

To take into account the effect of the mistag rate ω, we simply multiply the terms proportional to $\sin(\Delta\mathrm{m_s})$ or $\cos(\Delta\mathrm{m_s})$ in the $\mathrm{K_j(t)}$ functions defined in Equ. 36, with a coefficient $((1 - 2\omega) \times \mathrm{I_{cat}})$. Using the amended $\mathrm{K_j(t)}$ functions, Equ. 33 gives the flavour-tagged time-dependent angular distribution $\mathrm{p}^{\mathrm{tag}}_{\mathrm{sig}}(\mathrm{t}, \cos\theta_1, \cos\theta_2, \varphi, \mathrm{I_{cat}})$. The function $\mathrm{p}^{\mathrm{4D}}_{\mathrm{sig}}(\mathrm{t}, \cos\theta_1, \cos\theta_2, \varphi, \mathrm{I_{cat}})$ is a convolution of the PDF $\mathrm{p}^{\mathrm{tag}}_{\mathrm{sig}}(\mathrm{t}, \cos\theta_1, \cos\theta_2, \varphi, \mathrm{I_{cat}})$ with a Gaussian distribution of the proper time with mean 0 and width 42 fs. The function $\mathrm{p}^{\mathrm{mass}}_{\mathrm{sig}}(\mathrm{m_{B^0_s}})$ is a Gaussian distribution of the reconstructed $\mathrm{B^0_s}$ mass centered at the nominal $\mathrm{B^0_s}$ mass and with width 12 MeV/c^2.

$\mathrm{p}^{\mathrm{4D}}_{\mathrm{bg}}(\mathrm{t}, \cos\theta_1, \cos\theta_2, \varphi, \mathrm{I_{cat}})$ is constant with regard to $(\cos\theta_1, \cos\theta_2, \varphi, \mathrm{I_{cat}})$ and has an exponential dependence on time: $\mathrm{p}^{\mathrm{4D}}_{\mathrm{bg}}(\mathrm{t}, \cos\theta_1, \cos\theta_2, \varphi) \propto \mathrm{e}^{-\Gamma_{\mathrm{bg}}\mathrm{t}}$. Γ_{bg} is found to be 1.85 ps^{-1} in the full simulation. $\mathrm{p}^{\mathrm{mass}}_{\mathrm{bg}}(\mathrm{m_{B^0_s}})$ is a flat distribution.

The acceptance function for both signal and background has the form

$$\epsilon^{\mathrm{A}}_{\mathrm{sig(bg)}}(\mathrm{t}) \propto \frac{\mathrm{t}^3}{\mathrm{b_{sig(bg)}} + \mathrm{t}^3}. \tag{42}$$

The parameters and their input values used in the study are[3]

- number of signal events: 4 k, corresponding to 2.6 fb^{-1} of data;
- B/S: 0.9;
- ϕ_s: 0.2;
- $\mathrm{R}_\perp \equiv |\mathrm{A}_\perp|^2/(|\mathrm{A}_0|^2 + |\mathrm{A}_\parallel|^2 + |\mathrm{A}_\perp|^2)$: 0.25;

[3] Some input numbers used for the sensitivity study are not exactly the same as those described in the previous section as the event preselection study evolves but the changes may not be reflected in the sensitivity study. We will show how the statistical error of ϕ_s depends on input values of parameters such as $\mathrm{B^0_s} \to \phi\phi$ branching ratio. Compared with the experimental error of $\mathrm{B^0_s} \to \phi\phi$ branching ratio, uncertainties of other input parameters are expected to have much smaller effects on our fast simulation results.

- $R_{\|} \equiv |A_{\|}|^2/(|A_0|^2 + |A_{\|}|^2 + |A_{\perp}|^2)$: 0.25;
- $\delta_1 \equiv \arg(A_{\perp}/A_{\|})$: 0;
- $\delta_2 \equiv \arg(A_{\perp}/A_0)$: π;
- $\Gamma_s = (\Gamma_L + \Gamma_H)/2$: 0.67 ps^{-1};
- $\Delta\Gamma_s/\Gamma_s = (\Gamma_L - \Gamma_H)/\Gamma_s$: 0.15;
- Δm_s: 17.0 ps^{-1};
- signal proper time acceptance parameter b_{sig}: 0.027 ps^3;
- background proper time acceptance parameter b_{bg}: 1.2×10^{-4} ps^3;
- background lifetime parameter τ_{bg}: 0.54 ps;
- proper time resolution: 42 fs;
- B_s^0 mass resolution: 12 MeV/c^2;
- tagging efficiency 0.6;
- mistag rate 0.3.

In the fit ϕ_s, B/S, $R_{\perp}$, $R_{\|}$, δ_1, δ_2, Γ_s and $\Delta\Gamma_s/\Gamma_s$ are free parameters. The range of ϕ_s is chosen in a way to ignore the ambiguity caused by $\Gamma_H \Leftrightarrow \Gamma_L$, $\delta_1 \Rightarrow \pi - \delta_1$, $\delta_2 \Rightarrow \pi - \delta_2$ and $\phi_s \Rightarrow \pi - \phi_s$.

4.4 Sensitivity

We performed 500 toy experiments with $\phi_s^{input} = 0.20$ and obtained a statistical error $\sigma(\phi_s) = 0.100$ using a Gaussian fit to the distribution of ϕ_s^{fit} (Fig. 10). The corresponding pull distribution is also shown.

The distribution of $R_{\perp}^{fit}$ for $R_{\perp}^{input} = 0.25$ and the pull distribution of $R_{\perp}$ are shown in Fig. 11. The statistical error on $R_{\perp}$ is 0.012.

The distribution of $R_{\|}^{fit}$ for $R_{\|}^{input} = 0.25$ and the pull distribution of $R_{\|}$ are shown in Fig. 12. The statistical error on $R_{\|}$ is 0.014.

A Gaussian fit is applied to the pull distribution of ϕ_s, $R_{\perp}$ and $R_{\|}$ respectively. In all the three cases the fit result shows a mean value consistent with zero and a width consistent with one.

The dependence of $\sigma(\phi_s)$ on ϕ_s, $\Delta\Gamma_s/\Gamma_s$, $R_{\perp}$, $R_{\|}$, $\delta_1, \delta_2, \sigma(t)$, $\sigma(m_{B_s^0})$, B/S and $BR(B_s^0 \to \phi\phi)$ are shown in Table 4. It can be seen that $\sigma(\phi_s)$ strongly depends on $BR(B_s^0 \to \phi\phi)$ and slightly depends on $\Delta\Gamma_s/\Gamma_s$, but is not correlated with the other parameters.

The above results correspond to 2.6 fb^{-1} of data. Scaling to nominal luminosities gives $\sigma(\phi_s) = 0.11$ for 2 fb^{-1} of data and $\sigma(\phi_s) = 0.05$ for 10 fb^{-1} of data.

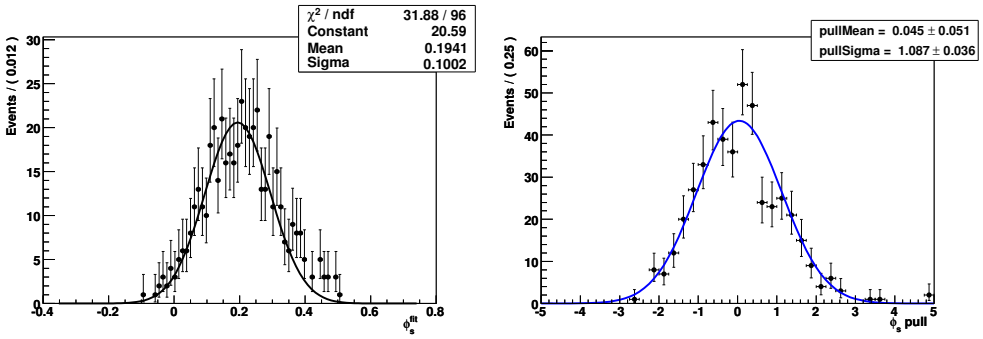

Figure 10 Left: the distribution of $\phi_{\rm s}^{\rm fit}$ for $\phi_{\rm s}^{\rm input} = 0.20$ from 500 toy experiments; right: the corresponding pull distribution.

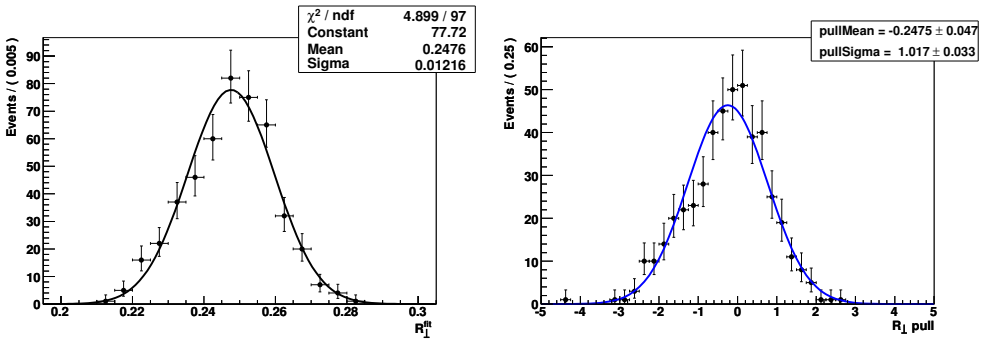

Figure 11 Left: the distribution of $\mathrm{R}_{\perp}^{\rm fit}$ for $\mathrm{R}_{\perp}^{\rm input} = 0.25$ from 500 toy experiments; right: the corresponding pull distribution.

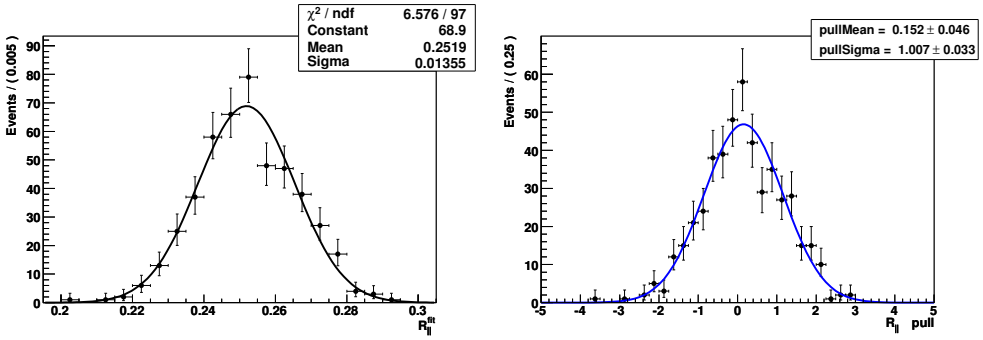

Figure 12 Left: the distribution of $\mathrm{R}_{\parallel}^{\rm fit}$ for $\mathrm{R}_{\parallel}^{\rm input} = 0.25$ from 500 toy experiments; right: the corresponding pull distribution.

5 Conclusions

The hadronic $b \to s$ penguin decay $\mathrm{B_s^0} \to \phi\phi$ is very sensitive to NP with extra CP phases. The event selection of this channel is described in this note. About 3.1 k events are expected in 2 fb^{-1} of data with $B/S < 0.8$ at 90% CL. Assuming the SM is valid, the total weak phase ϕ_s can be measured with precision of $\sigma(\phi_\mathrm{s}) = 0.11$ using 2 fb^{-1} of data. A measurement of ϕ_s significantly different from zero would imply new CP-violating phases in the penguin decay and/or $\mathrm{B_s^0}$ mixing and be a clear signal of NP. After about 5 years of data taking, LHCb is expected to accumulate a data sample of 10 fb^{-1} which will give a statistical uncertainty of $\sigma(\phi_\mathrm{s}) = 0.05$.

6 References

[1] R. Fleischer, hep-ph/0405091.

[2] Heavy Flavour Averaging Group, http://www.slac.stanford.edu/xorg/hfag/.

[3] M. Raidal, Phys. Rev. Lett. **89**, 231803 (2002).

[4] D. Acosta *et al.*, Phys. Rev. Lett. **95**, 031801 (2005).

[5] M. Beneke *et al.*, hep-ph/0612290.

[6] X. Li *et al.*, Phys. Rev. **D68**, 114015 (2003); Erratum-ibid. **D71**, 019902 (2005); hep-ph/0309136.

[7] D. Du and L. Guo, J. Phys. G: Nucl. Part. Phys. **23**, 525 (1997).

[8] Y.H. Chen *et al.*, Phys. Rev. **D59**, 074003 (1999).

[9] M. Calvi *et al.*, "Flavour Tagging Algorithms and Performances in LHCb", LHCb note 2007-058.

[10] W.-M Yao *et al.*, *Review of Particle Physics*, J. Phys. G, **33** (2006).

[11] S. Nandi *et al.*, J.Phys. **G32**, 835 (2006).

[12] Q. Chang *et al.*, hep-ph/0610280.

[13] M. Bauer *et al.*, Z. Phys. **C29**, 637 (1985); Z. Phys. **C34**, 103 (1987).

[14] A. Datta *et al.*, Phys. Rev. **D71**, 096002 (2005).

[15] A. Datta *et al.*, Phys. Lett. **B595**, 453 (2004).

Table 4 Dependence of $\sigma(\phi_s)$ on various parameters with 2.6 fb^{-1} of data.

Dependence of $\sigma(\phi_s)$ on ϕ_s				
ϕ_s	-0.2	0	0.2	0.4
$\sigma(\phi_s)$	0.107	0.098	0.100	0.092

Dependence of $\sigma(\phi_s)$ on $\Delta\Gamma_s/\Gamma_s$			
$\Delta\Gamma_s/\Gamma_s$	0.05	0.15	0.25
$\sigma(\phi_s)$	0.107	0.100	0.085

Dependence of $\sigma(\phi_s)$ on $R_\perp$			
$R_\perp$	0.15	0.25	0.35
$\sigma(\phi_s)$	0.101	0.100	0.097

Dependence of $\sigma(\phi_s)$ on $R_\parallel$			
$R_\parallel$	0.15	0.25	0.35
$\sigma(\phi_s)$	0.104	0.100	0.100

Dependence of $\sigma(\phi_s)$ on δ_1, δ_2			
δ_1, δ_2	$\pi/4, 3\pi/4$	$0, \pi$	$0, \pi/2$
$\sigma(\phi_s)$	0.099	0.100	0.100

Dependence of $\sigma(\phi_s)$ on $\sigma(t)$			
$\sigma(t)$	34 fs	42 fs	50 fs
$\sigma(\phi_s)$	0.092	0.100	0.105

Dependence of $\sigma(\phi_s)$ on $\sigma(m_{B_s^0})$			
$\sigma(m_{B_s^0})$	9 MeV/c^2	12 MeV/c^2	15 MeV/c^2
$\sigma(\phi_s)$	0.094	0.100	0.104

Dependence of $\sigma(\phi_s)$ on B/S				
B/S	0.5	0.9	2.0	5.0
$\sigma(\phi_s)$	0.098	0.100	0.106	0.126

Dependence of $\sigma(\phi_s)$ on $BR(B_s^0 \to \phi\phi)$				
$BR(B_s^0 \to \phi\phi)$ (10^{-5})	0.35	0.7	1.4	2.1
$\sigma(\phi_s)$	0.22	0.143	0.100	0.080

A High Level Trigger Criteria for $\mathrm{B_s^0} \to \phi\phi$

The following critera are used to select $\mathrm{K}^{\pm}$ candidates:

- Transverse momentum $\mathrm{P_t} > 300\,\mathrm{MeV}/c$;
- Momentum $\mathrm{P} > 2000\,\mathrm{MeV}/c$;
- Impact parametr significance $\mathrm{IP}/\sigma > 2$ with regard to all primary vertices.

The following critera are used to select $\phi \to \mathrm{K}^+\mathrm{K}^-$ candidates:

- $|\mathrm{M}(\mathrm{K}^+\mathrm{K}^-) - \mathrm{M}(\phi)| < 20\,\mathrm{MeV}/c^2$ where $\mathrm{M}(\phi)$ is the nominal mass of ϕ;
- Vertex $\chi^2 < 49$.

The following critera are used to select $\mathrm{B_s^0} \to \phi\phi$ candidates:

- $|\mathrm{M}(\phi\phi) - \mathrm{M}(\mathrm{B_s^0})| < 500\,\mathrm{MeV}/c^2$ where $\mathrm{M}(\mathrm{B_s^0})$ is the nominal mass of $\mathrm{B_s^0}$;
- Vertex $\chi^2 < 49$;
- $\mathrm{F} > 1\ \mathrm{mm}$ and $\mathrm{F}/\sigma_{\mathrm{F}} > 6$ where F is the flight distance with regard to the primary vertex to which the $\mathrm{B_s^0}$ candidate has the smallest impact parameter significance and σ_{F} is its error;
- Impact parametr significance $\mathrm{IP}/\sigma < 6$ with regard to all primary vertices;
- $\cos(\theta) > 0.9995$ where θ is the angle between the momentum direction and the flight direction of the $\mathrm{B_s^0}$ candidate.